Journal of Nepal Geological Society, 2022, Vol. 63, pp. 99–108
https://doi.org/10.3126/jngs.v63i01.50845

Landslide susceptibility mapping of the Main Boundary Thrust (MBT) region in Tinau-Mathagadhi Section of Palpa District, Lumbini Province

Kabi Raj Paudyal* and Rupendra Maharjan
Central Department of Geology, Tribhuvan University, Kirtipur, Kathmandu, Nepal
**Corresponding author's email: paudyalkabi1976@gmail.com*

ABSTRACT

The study was carried out in Tinau-Mathagadhi section of Palpa District, Lumbini Province. The output of the landslide susceptibility analysis using frequency ratio (FR) is evaluated. Google Earth (CNES/Airbus and Maxar Technologies) Imagery of 50 cm spatial resolution was used to detect landslides. Data training and testing sampling was created using the landslide inventory. Eight causative factors were derived from topographic, geological, and land-use maps. The causative factors and training events were used to determine the FR ratings. The objective of present study is to address the effect of the Main Boundary Thrust (MBT) along with other important parameters in landslide susceptibility mapping. The integration of causative factors that assigned FR scores yielded the landslide susceptibility map. The validation of 79.6% was obtained using the ROC-AUC curve. Among eight causative factors, it was found that distance from the Main Boundary Thrust (MBT), aspect, land-use, and geology are dominating factors in the occurrence of the landslide. The FR method is based on a quantitative relationship between landslide inventory and landslide affecting factors. The method is valid for Tinau-Mathagadhi section and MBT is one of the causes of landslides in this area.

Keywords: Tinau-Mathagadhi, Main Boundary Thrust, landslide susceptibility, frequency ratio, validation

Received: 28 March 2022 **Accepted:** 16 August 2022

INTRODUCTION

Nepal's hilly regions are characterized by rough terrain, active seismicity, and monsoon rains, rendering them vulnerable to a variety of geohazards. Landslides are dynamic geohazards that can have catastrophic effects on long-term socio-economic development in mountainous terrains.

The presence of deep and steep river valleys in central Nepal is largely supported by the geomorphic and tectonic past of the Nepal Himalaya (Bell et al., 2021). There are many large-scale and small-scale landslides in these valleys. Earthquakes often pose a long-term threat to the slope's stability, particularly in seismically active areas like Nepal (Roback et al., 2018). The study area, Tinau-Mathagadhi is located in Palpa District, Nepal (Fig. 1). The topography of the area is highly dissected and roughly followed by the presence of thrust (MBT) which makes it susceptible to landslides. The altitude of the area ranges from 389 m to 1843 m and the total area under study is 59.57 sq. km. The study area is bounded by 83.491358 to 83.639506 longitudes and 27.799393 to 27.735617 latitudes. The study area can be accessed by the Siddhartha Rajmarg and many other local roads. It is additionally connected with numerous graveled streets and foot trails.

The climatic condition of the Tinau-Mathagadhi area is upper tropical to the sub-tropical zone. The driest month is December, with 22 mm/0.9 inches of precipitation. Most of the precipitation here falls in July, averaging 690 mm/27.2 inches. Due to steep slope, rugged topography, and the fragile rock condition, the Tinau-Mathagadhi area is susceptible to many slopes instabilities issues.

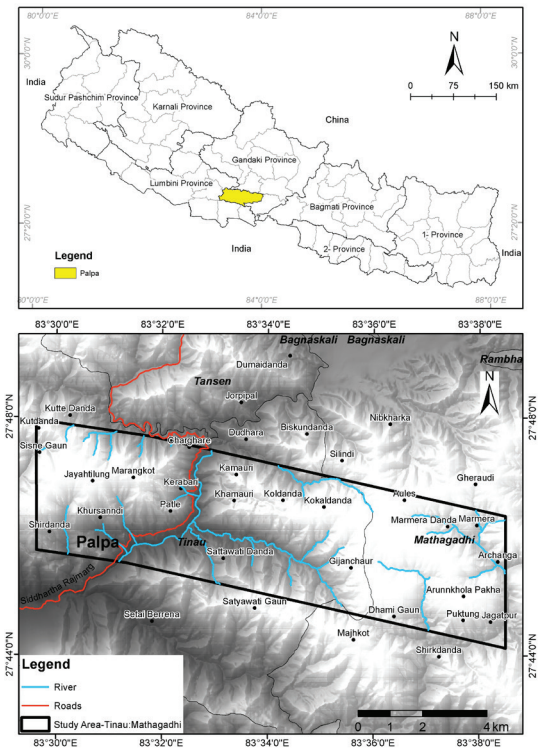

Fig. 1: Location map of the Tinau-Mathagadhi section.

METHODOLOGY

For landslide susceptibility mapping, it is critical to conclude that landslide causative factors affect the spatial distribution of landslides, and that future landslides will occur under similar conditions to previous landslides (Mersha and Meten, 2020).

Many researchers have devised efficient methods for creating an accurate landslide susceptibility map over the last few decades. Frequency ratio (Goetz et al., 2015; Hong et al., 2016; Lee et al., 2016), logistic regression (Chen et al., 2017; Steger et al., 2016), decision trees (Beucher et al., 2019), fuzzy logic (Pham et al., 2021), neuro-fuzzy systems (Shihabudheen and Pillai, 2018), support vector machines (Huang and Zhao, 2018), artificial neural networks (Gameiro et al., 2021), Analytical Hierarchy Process (AHP) (Sonker et al., 2021), information value method (IVM) (Farooq and Akram, 2021) and multimethod approach (Wubalem, 2021) are a few illustrations of these methods. The methodology used a frequency ratio (FR) to evaluate the efficiency of the landslide susceptibility study.

The FR model has the advantage of being able to rank the causative variables in terms of their likelihood of causing a landslide, as well as determining whether a given set of causative factor values would be dangerous in the case of a landslide.

Manual digitization of aerial photographs/satellite images from the Google Earth (March 2020) image was used to conduct the landslide inventory of 118. The inventory of landslides was then divided into training (70–83%) and testing (30–35%) samples. A training sample was used to create the landslide susceptibility index model (LSI) while a testing sample was used to validate the model by using Receiver Operating Curve (ROC). Figure 2 shows the detailed methodology used in the analysis.

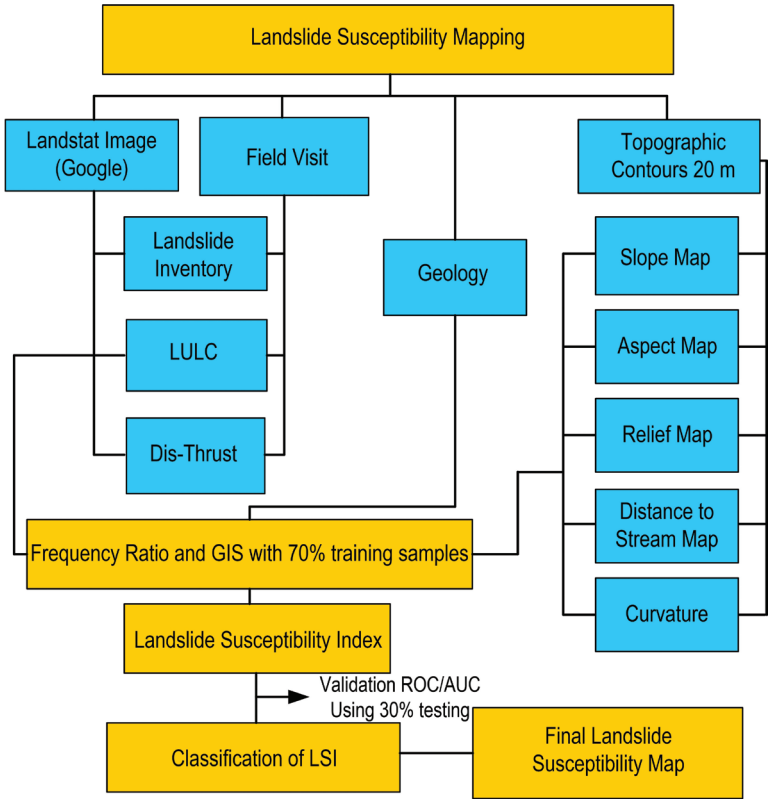

Fig. 2: Methodology of landslide susceptibility mapping by using FR method.

Landslide susceptibility mapping requires the preparation of thematic data layers. Hence eight thematic layers viz. geology, slope, aspect, plan curvature, distance from the stream, distance from the thrust (MBT), relief and land use land cover all of 20×20 m cell were used. A digital elevation model (DEM) derived from a triangulated irregular network (TIN) surface was used to prepare topographic and hydrologic factors. The TIN was generated using ArcMap 10.4.1 and contour lines at 20 m intervals from digital topographic maps. Topographic and hydrologic factors such as slope gradient, plan curvature, slope aspect, relief, distance from the stream were taken into account for landslide susceptibility. LULC map was prepared by digitizing the image in ArcMap10.4.1. Geology and MBT of the area were extracted from petroleum block (Department of Mines and Geology, Government of Nepal) data. Distance to MBT map was created using the Euclidean distance algorithm.

After preparing eight factor maps, a landslide inventory map was used to cross with the all-factor maps and generate tabulated data. Hence, landslide susceptibility mapping was carried out using the frequency ratio method (FRM). LSI map

so generated was classified into map into five zones viz. very low, low, moderate, high and very high susceptible zones.

Frequency ratio method

Understanding the area-specific, physical conditions and processes for triggering the landslides is of significant importance to evaluate the probability of landslides. Frequency ratio is a quantitative technique for landslide susceptibility assessment using GIS techniques and spatial data (Baral et al., 2021). The frequency ratio (FR) technique is frequently and effectively used for landslide susceptibility mapping (Wang and Li, 2017). It is based on the quantified association between the landslide inventory and the landslide causative factors (Saravanan et al., 2021). To obtain the frequency ratio (FR) for each class of the causative factors, a combination has been established between the landslide inventory map and factor map using Eq. (1) (Acharya and Lee, 2019; Fayez et al., 2018; Shu et al., 2021).

$$FR = \frac{Npix(1)/Npix(2)}{\sum Npix(3)/\sum Npix(4)} \quad (1)$$

where, Npix(1) = The number of pixels containing Landslide in a class, Npix(2) = Total number of pixels of each class in the whole area, Npix(3) = Total number of pixels containing landslide., Npix(4) = Total number of pixels in the study area

The derived frequency ratio is summed to develop a Landslide Susceptibility Index (LSI) map using Eq. (2) (Fayez et al., 2018).

$$LSI = FR_1 + FR_2 + FR_3 + FR_4 + \ldots\ldots\ldots + FR_n \quad (2)$$

RESULT AND DISCUSSION

Landslide inventory

Based on the Landsat images freely available on google earth and field visits, 118 landslides were mapped with a total area of 1.45 km^2 (Fig. 3a,b).

Influencing factors

Land-use/land-cover: Land cover map was prepared by using an image classification tool (Fig. 4a). Table 1 shows that forest occupies 62% of total area, agricultural land occupies 19.3%, barren land occupies 9.2%, 7.4% grassland, 1.1% water body, and 0.9% road of total area. The settlement occupies the least area of 0.2% only. Crossing LULC data with present landslide shows that 46.3% of total landslide lies in the barren land, 40.9% in forest area, 8.8% in grassland, 2.5% in agricultural land, and 0.4% of total landslide lies in the road (Table 1).

The frequency ratio for the land-use/land-cover shows that the barren land and grassland are highly susceptible to landslide as the high-frequency ratio are 5.05 and 1.18 respectively compared to other classes like the forest, settlement, and agricultural land which has least FR of 0.66, 0 and 0.13 respectively (Table 2).

Geology: A geological map from the department of mines and geology was used (Fig. 4b). Geologically, the study area is divided into five major groups viz. LS: Lower Siwalik, MS1: Lower Middle Siwalik, MS2: Upper Middle Siwalik, Ar: Aru Formation, and Ch: Charchare Formation. Table 1 shows that Aru Formation dominates the study area covering 52.5% of the total area whereas at the same geology 39.9% of total landslide is present. Maximum percentage (53.4%) of the landslide was observed in the Upper Middle Siwalik that occupies an area of 29.7%. Hence, MS2 region has a high-frequency ratio value of 1.8. The Lower Siwalik and Lower Middle Siwalik have the least frequency ratio and the FR of the Charchare Formation is 0 since the region occupies only 0.9% of the total study area and has no landslide in the vicinity.

Distance to thrust: Distance to thrust (MBT) is an extrinsic parameter considered in this study and is the most important landslide causative parameter (Nath et al., 2021). MBT from petroleum Block No. 5 was obtained from the Department of Mines and Geology, Government of Nepal. The block was then georeferenced and the location of MBT was traced from the map.

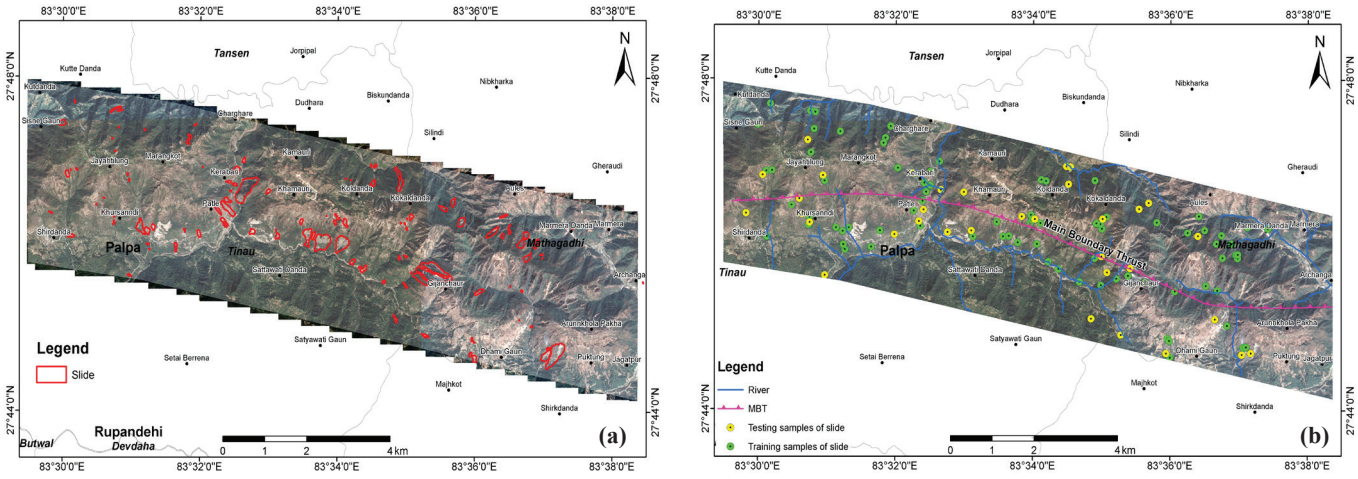

Fig. 3: Tinau-Mathagadhi section, Palpa District (a) Landslide inventory map, (b) Training and testing landslide datasets.

Table 1: Tabulation of domain with landslide inventory with areal coverage.

Domain	Class	Class Pixel	Area (sq. km)	% Class pixel	Landslide pixel	% Landslide pixel	Area (sq.km)
Slope	0 – 10°	5909	2.36	3.97	20	0.6	0.008
	10 – 20°	16225	6.49	10.90	82	2.3	0.033
	20 – 30°	35994	14.40	24.19	463	12.7	0.185
	30 – 40°	60193	24.08	40.45	1522	41.9	0.609
	40 – 50°	29013	11.61	19.50	1359	37.4	0.544
	50 – 61.8°	1483	0.59	1.00	186	5.1	0.074
Distance to Thrust	0 – 500 m	38280	15.31	25.7	1910	52.6	0.764
	500 – 1,000 m	37548	15.02	25.2	685	18.9	0.274
	1,000 – 1,500 m	37129	14.85	24.9	789	21.7	0.316
	1,500 – 2,000 m	27411	10.96	18.4	245	6.7	0.098
	2,000 – 2,640 m	8656	3.46	5.8	1	0.03	0.000
Land use	Agriculture	28728	11.49	19.3	90	2.5	0.036
	Grassland	11025	4.41	7.4	318	8.8	0.127
	Forest	92359	36.94	62.0	1485	40.9	0.594
	Barren Land	13660	5.46	9.2	1679	46.3	0.672
	Settlement	303	0.12	0.2	0	0.0	0.000
	Water Body	1585	0.63	1.1	44	1.2	0.018
	Road	1369	0.55	0.9	14	0.4	0.006
Geology	LS	2995	1.20	2.0	10	0.3	0.004
	Ar	78193	31.28	52.5	1450	39.9	0.580
	MS1	22301	8.92	15.0	231	6.4	0.092
	MS2	44249	17.70	29.7	1939	53.4	0.776
	Ch	1286	0.51	0.9	0	0.0	0
Distance to Stream	0 – 250 m	55529	22.21	37.3	1883	51.9	0.753
	250 – 500 m	44236	17.69	29.7	1247	34.4	0.499
	500 – 1000 m	42299	16.92	28.4	453	12.5	0.181
	1000 – 2300 m	6960	2.78	4.7	47	1.3	0.019
Curvature	Concave	68991	27.60	46.4	2128	58.6	0.851
	Linear	10217	4.09	6.9	207	5.7	0.083
	Convex	69609	27.84	46.8	1297	35.7	0.519
Aspect	North	21426	8.57	14.4	309	8.5	0.124
	Northeast	20398	8.16	13.7	268	7.4	0.107
	East	15047	6.02	10.1	180	5.0	0.072
	Southeast	17882	7.15	12.0	260	7.2	0.104
	South	22049	8.82	14.8	860	23.7	0.344
	Southwest	19255	7.70	12.9	668	18.4	0.267
	West	16481	6.59	11.1	620	17.1	0.248
	Northwest	16279	6.51	10.9	467	12.9	0.187
Relief	389 – 500 m	2937	1.17	2.0	22	0.6	0.009
	500 – 750 m	18783	7.51	12.6	1034	28.5	0.414
	750 – 1,000 m	33753	13.50	22.7	712	19.6	0.285
	1,000 – 1,250 m	45352	18.14	30.5	878	24.2	0.351
	1,250 – 1,500 m	35237	14.09	23.7	771	21.2	0.308
	1,500 – 1,843 m	12755	5.10	8.6	215	5.9	0.086

Table 2: Frequency ratio of each factor classes.

Domain	Class	Frequency Ration (FR)	Relative Frequency (RF)	RF (Non %)	Min RF	Max RF	Max-Min RF	(Max-Min) Min RF	PR
Slope	0 – 10°	0.14	0.02	1.55	0.02	0.21	0.20	0.14	1.43
	10 – 20°	0.21	0.02	2.31					
	20 – 30°	0.53	0.06	5.88					
	30 – 40°	1.04	0.12	11.55					
	40 – 50°	1.92	0.21	21.40					
	50 – 61.8°	5.14	0.57	57.31					
Distance to Thrust	0 – 500 m	2.05	0.51	50.68	0.00	0.51	0.51	0.14	3.63
	500 – 1,000 m	0.75	0.19	18.53					
	1,000 – 1,500 m	0.87	0.22	21.59					
	1,500 – 2,000 m	0.37	0.09	9.08					
	2,000 – 2,640 m	0.005	0.001	0.12					
Land-use	Agriculture	0.13	0.01	1.50	0.00	0.59	0.59	0.14	4.22
	Grassland	1.18	0.14	13.80					
	Forest	0.66	0.08	7.69					
	Barren Land	5.05	0.59	58.82					
	Settlement	0.00	0.00	0.00					
	Water Body	1.14	0.13	13.29					
	Road	0.42	0.05	4.89					
Geology	LS	0.14	0.04	4.39	0.00	0.58	0.58	0.14	4.13
	Ar	0.76	0.24	24.38					
	MS1	0.43	0.14	13.62					
	MS2	1.80	0.58	57.61					
	Ch	0.00	0.00	0.00					
Distance to stream	0 – 250 m	1.39	0.43	42.62	0.08	0.43	0.34	0.14	2.45
	250 – 500 m	1.16	0.35	35.43					
	500 – 1000 m	0.44	0.13	13.46					
	1000 – 2300 m	0.28	0.08	8.49					
Curvature	Concave	1.26	0.44	44.23	0.27	0.44	0.18	0.14	1.26
	Linear	0.83	0.29	29.05					
	Convex	0.76	0.27	26.72					
Aspect	North	1	0.07	7.43	0.06	0.20	0.14	0.14	1.00
	Northeast	1	0.07	6.77					
	East	0.49	0.06	6.16					
	Southeast	0.60	0.07	7.49					
	South	1.60	0.20	20.10					
	Southwest	1.42	0.18	17.88					
	West	1.54	0.19	19.38					
	Northwest	1	0.15	14.78					
Relief	389 – 500 m	0.31	0.05	5.29	0.05	0.39	0.34	0.14	2.41
	500 – 750 m	2.26	0.39	38.84					
	750 – 1,000 m	0.86	0.15	14.88					
	1,000 – 1,250 m	0.79	0.14	13.66					
	1,250 – 1,500 m	0.90	0.15	15.44					
	1,500 – 1,843 m	0.69	0.12	11.89					

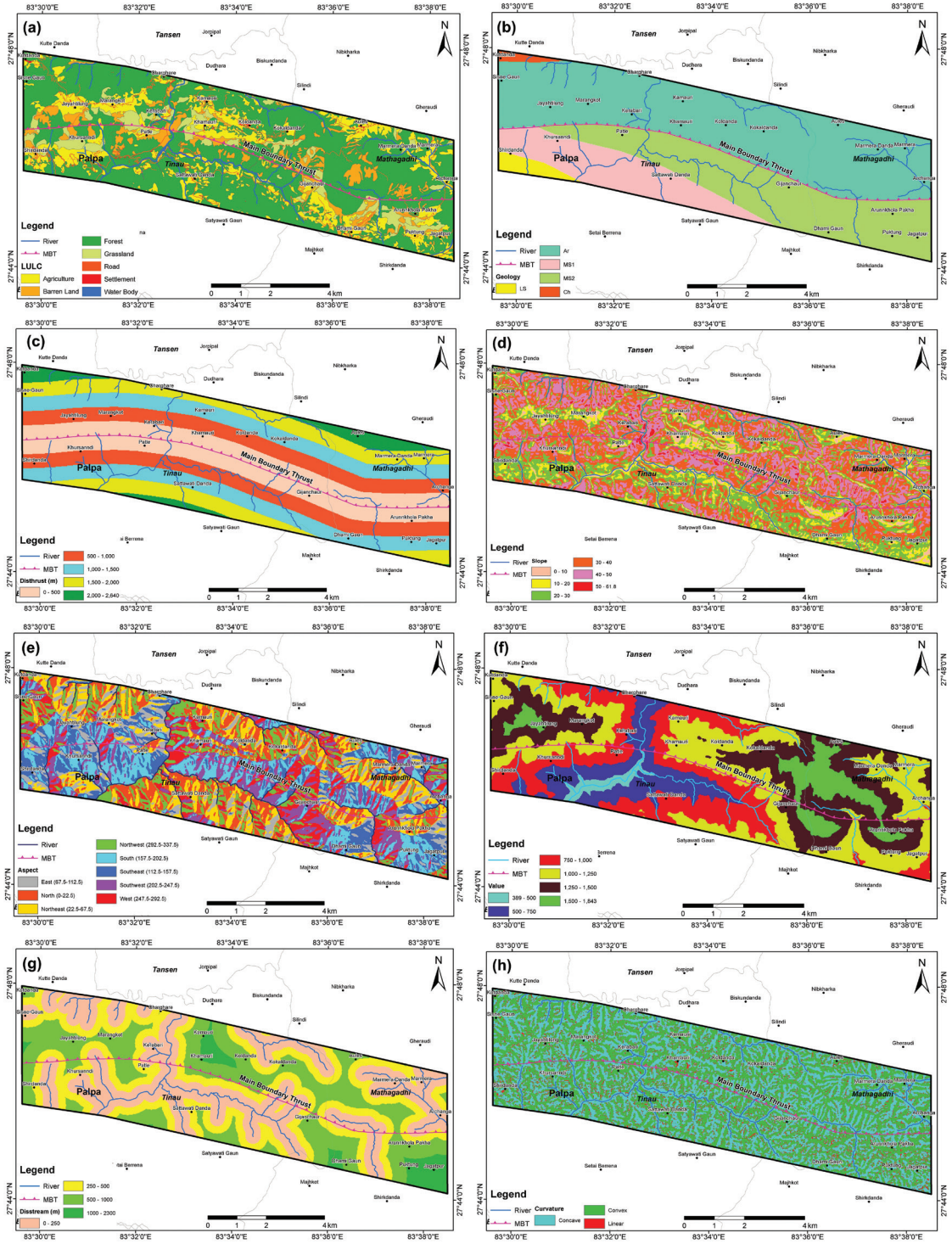

Fig. 4: a) Land-use map, b) Geological map, c) Distance to thrust (MBT) map, d) Slope map, e) Aspect map, f) Relief map, g) Distance to stream map, and h) Curvature map of the study area.

The distance to thrust (MBT) map was created using the MBT and Euclidean distance tool that describes each cell's relationship to a source or a set of sources based on the straight-line distance (Fig. 4c). The map was categorized into five divisions at an interval of 500 m. It was found that the nearest distance i.e., 0–500 m was the most vulnerable zone to landslides since the maximum percentage (52.6%) of all the landslides was found to be accumulated in this zone, this statement is also supported by the Frequency Ratio table as the zone has the highest FR value of 2.05.

Slope: Slope map was generated using 20×20 m Digital Elevation Model (DEM) using the algorithm slope of Surface-Spatial Analyst Tool in ArcMap (Fig. 4d). The slope is classified into six classes using the equal interval classification method.

Table 1 shows that the slope angle ranged 0–20° occupies the area of 3.97% of the total study area and has 0.6% of total landslide in it. Similarly slope angle ranged 10–20°, 20–30°, 30–40°, 40–50°, 50–61.8° occupies 10.9%, 24.19%, 40.45%, 19.5% and 1% of total study area respectively and landslide in the respective slopes are 2.3%, 12.7%, 41.9%, 37.4% and 5.1%. The terrain with a slope of 50–61.8° is most prone to landslides with a frequency ratio of 5.14 and the terrain with a slope gradient of $<10^0$ is least prone to landslides with a frequency ratio of 0.14 (Table 1).

Aspect: Aspect map was prepared using 20×20 m DEM using the algorithm aspect of Surface-Spatial Analyst Tool in ArcMap (Fig. 4e). The aspect was classified into eight classes (Table 1). It is found that a south-facing slope that occupies 14.8% of the total study area dominates the study area. The second and third dominant aspects are north and northeast facing aspects respectively. Most of the landslides were observed in these aspects i.e., south (23.7%), southwest (18.4%), west (17.1%), and northwest (12.9%). The frequency ratio for the aspect map shows that the south, west & south-west facing aspect has the highest frequency ratio value of 1.6, 1.54 and 1.42 respectively (Table 1), and are comparably more prone to landslides.

Relief: A relief map or elevation map of the study area was generated using 20×20 m DEM (Fig. 4f). The lowest elevation is observed as 389 m and the highest elevation is 1843 m. The relief map was classified into six classes (Table 1). It was observed that the elevation ranged 500–750 m occupies 12.6% of the total study area and has 28.5% of total landslides with the highest frequency ratio of 2.26.

Distance from stream: Stream is one of the important factors of landslide susceptibility mapping. The ground near the stream is more prone to landslide, hence the distance to the stream map (Fig. 4g) was generated using the Euclidean distance tool that describes each cell's relationship to a source or a set of sources based on the straight-line distance. It is classified into four interval classes. Table 1 shows that the vicinity in the range of 0 to 250 m covers 37.3 % of the total study area and covers 58.6% of total landslide. Also, the area ranging distance of 0–250 m from the streams has a high-frequency ratio of 1.39 and is prone to landslides in the future too.

Curvature: The curvature is the amount by which a curve deviates from being a straight line, or a surface deviates from being a plane (Fig. 4h). The curvature map was prepared using 20×20 m DEM using the algorithm aspect of Surface-Spatial Analyst Tool in ArcMap. Curvature is categorized into concave, linear, and convex surfaces. Table 1 shows that the study area is more convex by 46.8% of the total area whereas 46.4% of the total area is of concave topography and the remaining 6.9% is linear or plane surface. Most of the landslide has occurred on the concave surface as 58.6% of the total landslide lies in this zone. Thus, concave is more prone to a landslide which is also supported by the frequency ratio that value 1.26.

Landslide susceptibility analysis

Landslide susceptibility Index map (LSI) was prepared by combining all eight factor maps (Eq. 3) (Fig. 5).

$$LSI = PR_{d1} \times FR_1 + PR_{d2} \times FR_2 + PR_{d3} \times FR_3 + PR_{d4} \times FR_4 + \ldots . \ldots . + PR_{dn} \times FR_n \quad (3)$$

where, PR = Predictive ratio of each domain, FR = Frequency ratio of each class of a domain (Influencing Factors).

Here the predictive ratio (Table 3) is the weight given to the domain or the influencing factor from Table 1, which is calculated as in Equation 4:

$$PR = (Max\ RF – Min\ RF)/ (Min\ RF\ of\ Max\ RF – Min\ RF) \quad (4)$$

where, *RF* stands for relative frequency. It is the ratio of *FR* of a class of a domain to the total FR of the domain.

LSI was created by using the Eq. (2). For the classification of LSI data, ROC/AUC curve was used (Fig. 6). To check the predictive power of the proposed frequency method for landslide potential zone, LSI (landslide susceptibility index) was examined by success rate curves**.**

Figure 6 shows the area under the success rate curve (ROC/AUC) is 0.796, indicating that the prediction rate was 79.6% and 80.4% as upper bound, the analysis is valid. For the landslide potential, the success rate reveals that 20% of the study area, has a high rank and could explain 65% of the total landslide of the area. Likewise, 40% and 50% of proposed GWP values could explain around 78% and 85% of all existing landslide respectively. Finally, three Groundwater Potential classes are established as Very low susceptibility (greater than 50%), low susceptibility (40–50%), moderate susceptibility (20–40%), high susceptibility (10–20%)**,** and very high susceptibility (0–10%) using which final landslide susceptibility map is prepared.

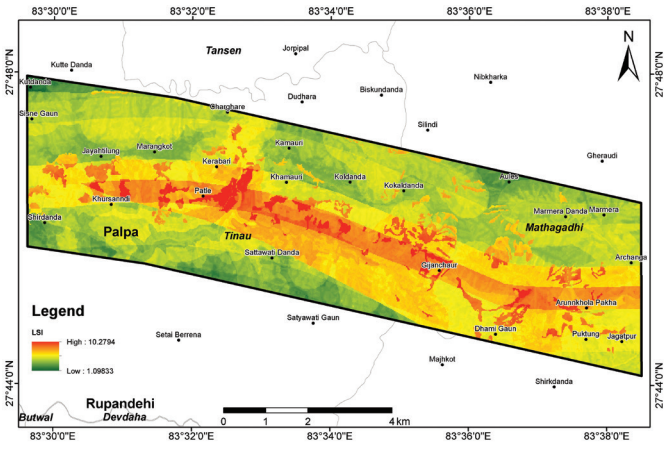

Fig. 5: Landslide susceptibility index map of the study area.

Table 3: Weight of individual factor.

Domain/Factor	PR	Weight
Aspect	1.00	100
Curvature	1.26	126
Slope	1.43	143
Relief	2.41	241
Distance to stream	2.45	245
Distance to thrust	3.63	363
Geology	4.13	413
Land-use	4.22	422

Hence, the LSI was classified into five susceptibility zones viz. very low, low, moderate, high, and very high susceptibility zones with the threshold value of respective classes are 4.26, 4.74 5.79, 6.65, and 10.28 respectively (Table 4) using which final landslide susceptibility maps was prepared (Fig. 7).

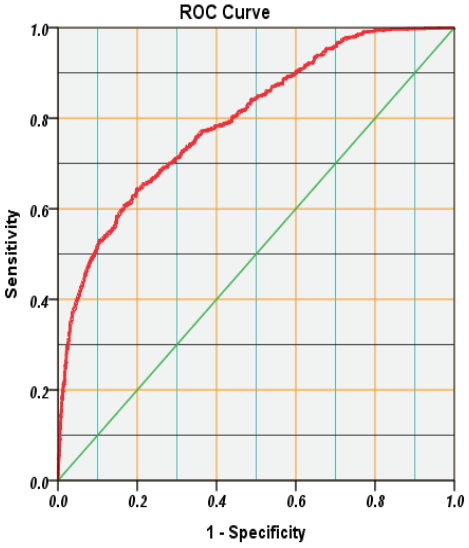

Fig. 6: ROC/AUC Curve of landslide susceptibility assessment in Tinau-Mathagadhi.

Table 4: Boundary value set for different susceptibility classes.

Cumulative (%)	Susceptible Class	LSI *Upper Bound*
50%	Very Low	4.26
60%	Low	4.74
80%	Moderate	5.79
90%	High	6.65
100%	Very	10.28

The result of the final susceptibility map prepared using eight influencing factor maps suggests that Patle village lies in a very high susceptibility zone and is a prone area (Fig. 8). Arun Khola Pakha, Gijanchaur, and Kerabari lie in the high susceptibility zone. The rest of the villages i.e. lie in either low or very low susceptible zone. Out of the total study area, 60% of the area is stable (Shirdanda, Jayahtilung, Sisne Gaun, Marangkot, Charghare, Kamauri, Khamauri, Sattawati Danda, Kholdanda, Kokaldanda, Aules, Dhami Gaun, Marmera Danda, Archanga, Puktung, and Jagatpur) while 20% is moderately susceptible and 10% region of the study area is highly and 10% is very highly prone to landslides in near future (Fig. 7, 8; Table 5).

Table 5: Area coverage by different landslide susceptibility classes.

Landslide Susceptibility				Landslide	Classification Method
Suseptible Class	Count	Area (sq.km)	Area (%)	(%)	
Very Low	74144	29.66	50%	15.21 %	ROC/AUC Curve
Low	14682	5.87	10%	6.45 %	
Moderate	29893	11.96	20%	14.16 %	
High	14783	5.91	10%	12.64 %	
Very high	14844	5.94	10%	51.54 %	
Total	148346	59.34	100%	15.21 %	

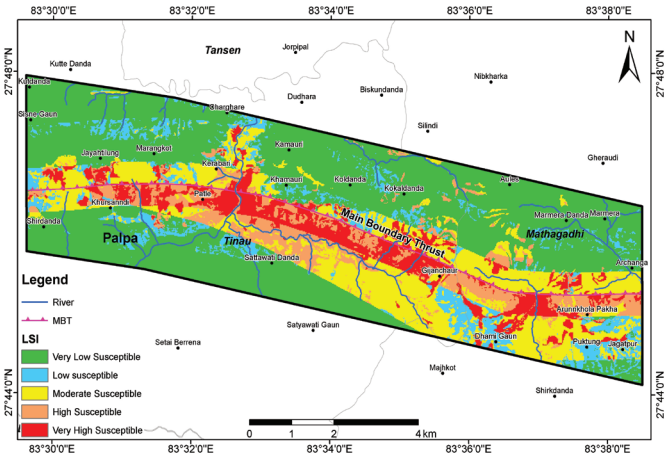

Fig. 7: Landslide Susceptibility map of the Study area (Tinau-Mathagadhi).

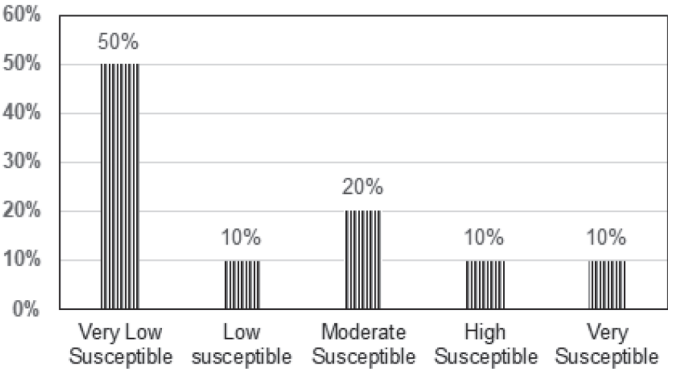

Fig. 8: The percentage of susceptibility class in Tinau-Mathagadhi.

DISCUSSIONS

Landslide causative factors

The contributing factors were selected in this study based on the presence or absence of the factors and their importance. The landslide conditioning factors incorporated the geomorphological, anthropogenic, and extrinsic factors. In this study, eight conditioning factors were considered to prepare the landslide susceptibility map namely, distance from a thrust (MBT), aspect, slope, land use land cover, relief, distance from the stream, geology, and curvature.

The frequency ratio values showed that the terrain slope has a significant impact on the landslide distribution. Generally, occurrences of landslides increase with an increase in terrain gradient. This statement is also supported by our analysis since the slope of 50°–61.8° gradient has the highest FR value of 5.14 and is most prone the landslides. the terrain with a slope

gradient of $<10^0$ is least prone to landslides with a frequency ratio of 0.14. The frequency ratio for the aspect map shows that the South, Southwest, and west-facing aspect has the highest frequency ratio values. The south aspect has the maximum FR of 1.6 followed by the west with 1.54 and the south-west slope has an FR value of 1.42. The area range of 0–250 m from the streams has a high-frequency ratio of 1.39. Among the land-use/land-cover, the barren land has the highest FR of 5.05. It is found that concave curvature has a high frequency of landslide occurrence with the value of 1.26. Also, it was observed that that most of the landslides were occurring in the Upper Middle Siwalik zone with a frequency ratio of 1.8 followed by Aru Formation with FR of 0.76. The nearest distance from the thrust, MBT has the highest number of landslides with the highest frequency ratio value of 2.05; hence, the zone of 0–500 m distance is most vulnerable to landslide.

Topographic parameters

The DEM has been used as an important factor in the study of earthquake-induced landslides (Wang et al., 2015). Research shows an increase in the probability of landslide occurrence for higher elevation although there is an absence of any direct relationship between the elevation and landslide occurrence (Liu et al., 2021). The landslide concentration was maximum for elevation range 500–750 m. The steepness of the slope is another major topographic factor used in landslide susceptibility studies (Regmi et al., 2016). The slope ranges from 0–61.8°. The landslide concentration was maximum along with the slope range from 50–61.8°. The aspect of the slope resembles the moisture retention and its relation to the attitude of bedding of the rock formation which in turn affects the physical properties of slope material and its susceptibility to failure (Gadtaula and Dhakal, 2019). In this study, the aspect to the south, southwest, and west contributes mostly to landslides. It is usually because most of the river segments trend towards SW-SE and many landslides appear on the slope towards the river.

The surface undulation of the slope can play a major role in triggering landslides as it has a strong influence on creating slope instability. In curvatures, the landslides are usually distributed in convex slopes and concave slopes. The convex slopes usually have earthquake-induced landslides (Gadtaula and Dhakal, 2019).

Anthropogenic factor

Land-use is considered to be one of the landslide conditioning factors as the variation in the land-use might play a role in changing the vegetation cover varying the mechanical (e.g., soil strength and slope behavior) and hydrological (e.g. Roccati et al., 2021). The variation in land use distribution may be either natural, human-induced, or a combination of both. Land-use map was generated by manual digitization of satellite image (Google Earth Image) of the study area. The frequency ratio weight values depict that the correlation of barren land and grassland, that is 5.05 and 1.18 respectively is stronger than other land use classes and our result matches concerning the value obtained however the landslide was not found in barren lands.

CONCLUSIONS

In this study, the Frequency Ratio model based on statistical method was used for determining the spatial probability of landslide occurrence where each factor layer was weighted according to the contribution on landslides. This method predicted the probability of landslide occurrence efficiently which was validated by positive correlations between the field conditions and the results obtained by the model. A total of 118 landslides were identified. It is found that landslides are more influenced by distance from the thrust (MBT). Geology factor map suggests that most of the landslides have occurred in the Upper Middle Siwalik zone. The slope map exhibit that the landslides are more focused in the slope angle between 50° and 61.8°, the result shows landslide mostly occur in higher slopes or increasing relief. It was observed that the slope angle less than 10 degrees did not contribute much to induce landslides.

The results suggested that the landslides are most common in a slope facing south, southwest, and west. While the curvature suggested that concave curvature is the role player to predict landslides. During the study of elevation map, it suggested that the number of landslides increase until 750 m and then decline in area percentage of landslide.

The agricultural land followed by forest area and agricultural land covered the maximum area in the Tinau-Mathagadhi region but the result suggests that barren land is found to be vulnerable to landslide. It was found from the study that the distance from the thrust (MBT) had a direct correlation with the landslide event as the landslide distribution is maximum around the MBT zone ranging the distance of 0–500 m. The statistical analysis obtained from the results of the susceptibility map prepared by using the Frequency Ratio model gave the result that maximum area of landslide distribution was observed in very high susceptibility class or unstable zone i.e., 51.54%, high susceptibility zone has 12.64%, the moderate zone has 14.16%, low susceptibility and very low susceptibility zone have 21.66% combined. Among the different factors, aspects, distance from the thrust (MBT), land use, and geology were found to be the major contributors to trigger the landslides in the Tinau-Mathagadhi area.

ACKNOWLEDGEMENT

Authors are thankful with Rabindra Nepal, Pramod Kattel and Pradip Shrestha for accompanying the field.

REFERENCES

Acharya, T. D. and Lee, D. H., 2019, Landslide Susceptibility Mapping using Relative Frequency and Predictor Rate along Araniko Highway. KSCE Journal of Civil Engineering, 23(2), pp. 763–776.

Bell, R., Fort, M., Götz, J., Bernsteiner, H., Andermann, C., Etzlstorfer, J., Posch, E., Gurung, N., and Gurung, S. 2021, Major geomorphic

events and natural hazards during monsoonal precipitation 2018 in the Kali Gandaki Valley, Nepal Himalaya. Geomorphology, 372, 107451. https://doi.org/10.1016/j.geomorph.2020.107451

Beucher, A., Møller, A. B., and Greve, M. H., 2019, Artificial neural networks and decision tree classification for predicting soil drainage classes in Denmark. Geoderma, 352, pp. 351–359.

Chen, W., Xie, X., Wang, J., Pradhan, B., Hong, H., Bui, D. T., Duan, Z., and Ma, J., 2017, A comparative study of logistic model tree, random forest, and classification and regression tree models for spatial prediction of landslide susceptibility. CATENA, 151. https://doi.org/10.1016/j.catena.2016.11.032

Farooq, S. and Akram, M. S., 2021, Landslide susceptibility mapping using information value method in Jhelum Valley of the Himalayas. Arabian Jour. Geosci., 14(10), 824. https://doi.org/10.1007/s12517-021-07147-7

Fayez, L., Pazhman, D., Pham, B. T., Dholakia, M. B., Solanki, H. A., Khalid, M., and Prakash, I., 2018, Application of Frequency Ratio Model for the Development of Landslide Susceptibility Mapping at Part of Uttarakhand State, India. Inter. Jour. Applied Eng. Research, v. 13(9). http://www.ripublication.com

Gadtaula, A. and Dhakal, S., 2019, Landslide susceptibility mapping using Weight of Evidence Method in Haku, Rasuwa District, Nepal. Jour. Nepal Geol. Soc., 58, pp. 163–171.

Gameiro, S., Riffel, E. S., de Oliveira, G. G., and Guasselli, L. A., 2021, Artificial neural networks applied to landslide susceptibility: The effect of sampling areas on model capacity for generalization and extrapolation. Applied Geography, 137, 102598. https://doi.org/10.1016/j.apgeog.2021.102598

Goetz, J. N., Brenning, A., Petschko, H., and Leopold, P., 2015, Evaluating machine learning and statistical prediction techniques for landslide susceptibility modeling. Computers & Geosciences, 81. https://doi.org/10.1016/j.cageo.2015.04.007

Hong, H., Pourghasemi, H. R., and Pourtaghi, Z. S., 2016, Landslide susceptibility assessment in Lianhua County (China): A comparison between a random forest data mining technique and bivariate and multivariate statistical models. Geomorphology, 259. https://doi.org/10.1016/j.geomorph.2016.02.012

Huang, Y. and Zhao, L., 2018, Review on landslide susceptibility mapping using support vector machines. CATENA, 165, pp. 520–529.

Lee, M. J., Park, I., Won, J. S., and Lee, S. 2016, Landslide hazard mapping considering rainfall probability in Inje, Korea. Geomatics, Natural Hazards and Risk, 7(1). https://doi.org/10.1080/19475705.2014.931307

Liu, J., Wu, Y., and Gao, X., 2021, Increase in occurrence of large glacier-related landslides in the high mountains of Asia. Scientific Reports, 11(1), 1635. https://doi.org/10.1038/s41598-021-81212-9

Mersha, T. and Meten, M., 2020, GIS-based landslide susceptibility mapping and assessment using bivariate statistical methods in Simada area, northwestern Ethiopia. Geoenvironmental Disasters, 7(1), 20. https://doi.org/10.1186/s40677-020-00155-x

Nath, R. R., Das, N., and Satyam, D. N., 2021, Impact of Main Boundary Thrust (MBT) on Landslide Susceptibility in Garhwal Himalaya: A Case Study. Indian Geotech. Jour., 51(4), pp. 746–756.

Baral, N., Karna, A. K., and Gautam, S. 2021, Landslide Susceptibility Assessment Using Modified Frequency Ratio Model in Kaski District, Nepal. International Jour. Engineering and Management Research, 11(1), pp. 167–177.

Pham, Q. B., Achour, Y., Ali, S. A., Parvin, F., Vojtek, M., Vojteková, J., Al-Ansari, N., Achu, A. L., Costache, R., Khedher, K. M., and Anh, D. T., 2021, A comparison among fuzzy multi-criteria decision making, bivariate, multivariate and machine learning models in landslide susceptibility mapping. Geomatics, Natural Hazards and Risk, 12(1), 1741–1777. https://doi.org/10.1080/19475705.2021.1944330

Regmi, A. D., Dhital, M. R., Zhang, J., Su, L., and Chen, X., 2016, Landslide susceptibility assessment of the region affected by the 25 April 2015 Gorkha earthquake of Nepal. Jour. Mt. Sci., 13(11). https://doi.org/10.1007/s11629-015-3688-2

Roback, K., Clark, M. K., West, A. J., Zekkos, D., Li, G., Gallen, S. F., Chamlagain, D., and Godt, J. W., 2018, The size, distribution, and mobility of landslides caused by the 2015 Mw7.8 Gorkha earthquake, Nepal. Geomorphology, 301, 121–138. https://doi.org/10.1016/j.geomorph.2017.01.030

Roccati, A., Paliaga, G., Luino, F., Faccini, F., and Turconi, L., 2021, GIS-Based Landslide Susceptibility Mapping for Land Use Planning and Risk Assessment. Land, 10(2), 162. https://doi.org/10.3390/land10020162

Saravanan, S., Istijono, B., Jennifer, J. J., Abijith, D., and Sivaranjani, S. 2021, Landslide susceptibility assessment using frequency ratio technique – A case study of NH67 road corridor in the Nilgiris district, Tamilnadu, India. IOP Conference Series: Earth and Environmental Science, 708(1), 012017. https://doi.org/10.1088/1755-1315/708/1/012017

Shihabudheen, K. V. and Pillai, G. N., 2018, Recent advances in neuro-fuzzy system: A survey. Knowledge-Based Systems, 152, pp. 136–162.

Shu, H., Guo, Z., Qi, S., Song, D., Pourghasemi, H. R., and Ma, J., 2021, Integrating Landslide Typology with Weighted Frequency Ratio Model for Landslide Susceptibility Mapping: A Case Study from Lanzhou City of Northwestern China. Remote Sensing, 13(18), 3623. https://doi.org/10.3390/rs13183623

Sonker, I., Tripathi, J. N., and Singh, A. K., 2021, Landslide susceptibility zonation using geospatial technique and analytical hierarchy process in Sikkim Himalaya. Quaternary Science Advances, 4, 100039. https://doi.org/10.1016/j.qsa.2021.100039

Steger, S., Brenning, A., Bell, R., Petschko, H., and Glade, T., 2016, Exploring discrepancies between quantitative validation results and the geomorphic plausibility of statistical landslide susceptibility maps. Geomorphology, 262. https://doi.org/10.1016/j.geomorph.2016.03.015

Wang, L.-J., Guo, M., Sawada, K., Lin, J., and Zhang, J., 2015, Landslide susceptibility mapping in Mizunami City, Japan: A comparison between logistic regression, bivariate statistical analysis and multivariate adaptive regression spline models. CATENA, 135. https://doi.org/10.1016/j.catena.2015.08.007

Wang, Q. and Li, W., 2017, A GIS-based comparative evaluation of analytical hierarchy process and frequency ratio models for landslide susceptibility mapping. Physical Geography, 38(4). https://doi.org/10.1080/02723646.2017.1294522

Wubalem, A., 2021, Landslide susceptibility mapping using statistical methods in Uatzau catchment area, northwestern Ethiopia. Geoenvironmental Disasters, 8(1), 1. https://doi.org/10.1186/s40677-020-00170-y